PREDICTION OF FORMATION OF LAND-TIED ISLANDS

Shiho Miyahara[1], Takaaki Uda[2] and Masumi Serizawa[1]

When waves are incident to a sandy beach from two opposite directions, a cuspate foreland or a land-tied island may develop. A typical land-tied island can be seen offshore of Shodoshima Island in the Seto Inland Sea. Another example is Chiringashima Island located in the south part of Satsuma Peninsula, Kyushu. In both cases, the island and land are connected by an extremely slender sand bar that has been stably maintained for a long time, suggesting that it is stable against wave action from both sides of the sand bar. We developed a numerical model for predicting the elongation of a sand bar of a land-tied island using the BG model (a three-dimensional model for predicting beach changes based on Bagnold's concept).

Keywords: Land-tied island; BG model; beach changes; Shodoshima Island; Chiringashima Island

INTRODUCTION

When waves are incident to a sandy beach from two opposite directions, a cuspate foreland or a land-tied island may develop. A typical land-tied island can be seen offshore of Shodoshima Island in the Seto Inland Sea, Japan. This land-tied island extends from Bentenjima to Oyoshima Islands and incoporates two small islands, Nakayoshima and Shoyoshima islands, as shown in Figs. 1 and 2. Another example is Chiringashima Island located near the mouth of Kagoshima Bay in Kyushu, as shown in Fig. 3, and a narrow sand bar extends northeastward for 800 m from the Ibusuki coast to connect the island, as shown in Fig. 4. In both cases, the island and land are connected by an extremely slender sand bar that has been stably maintained for a long time, suggesting that it is stable against wave action from both sides of the sand bar. The sand bars connecting these islands are popular tourist attractions because of the beautiful scenery, and understanding their formation is important for their conservation. However, the formation of a land-tied island has not been predicted in previous studies, which have focused on describing the morphological features of the fully developed land-tied island, such as by Nagayama et al. (2009, 2010). In this study, field observations were carried out at the sand bars formed in the vicinity of Oyoshima and Chiringashima Islands, and then we developed a numerical model for predicting the elongation of a sand bar of a land-tied island using the BG model, which was originally proposed by Serizawa et al. (2006), and then was applied to the prediction of the deformation of a coral cay when detached breakwaters were constructed around a circular island (Sannami et al., 2013).

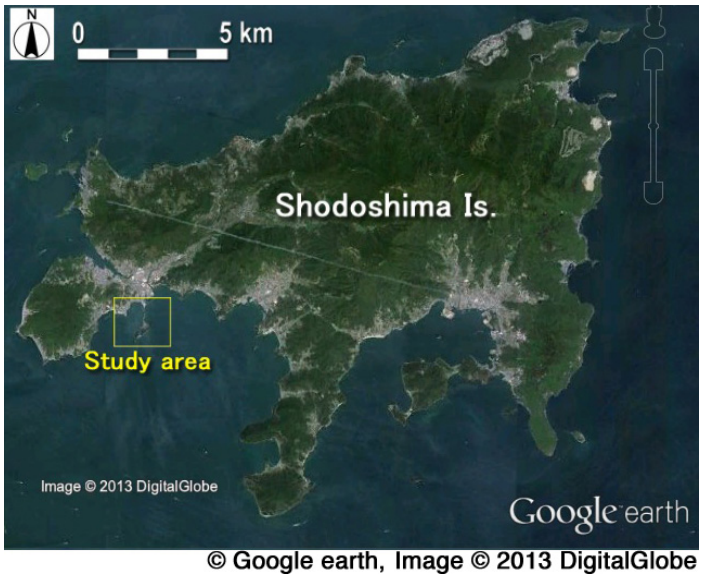

Figure 1. Location of study area on south shore of Shodoshima Island.

[1] Coastal Engineering Laboratory Co., Ltd., 1-22-301 Wakaba, Shinjuku, Tokyo 160-0011, Japan
[2] Public Works Research Center, 1-6-4 Taito, Taito, Tokyo 110-0016, Japan

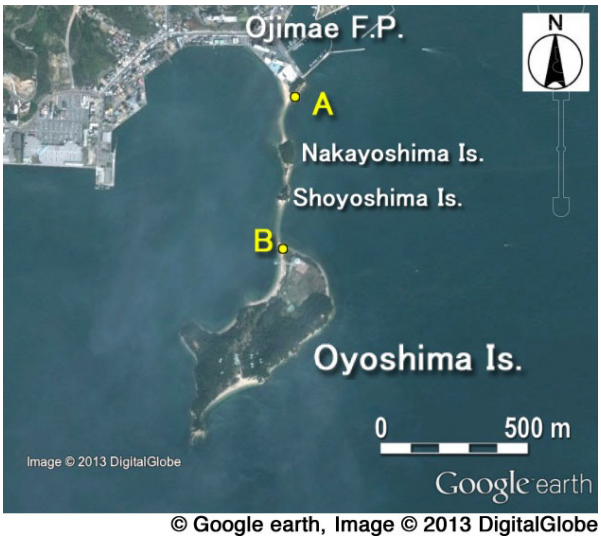

Figure 2. A sand bar of land-tied island extending between Shodoshima and Oyoshima Islands.

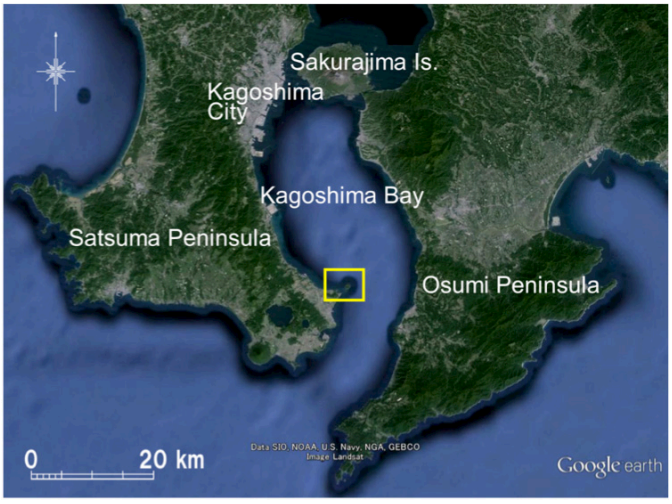

Figure 3. Study area near mouth of Kagoshima Bay.

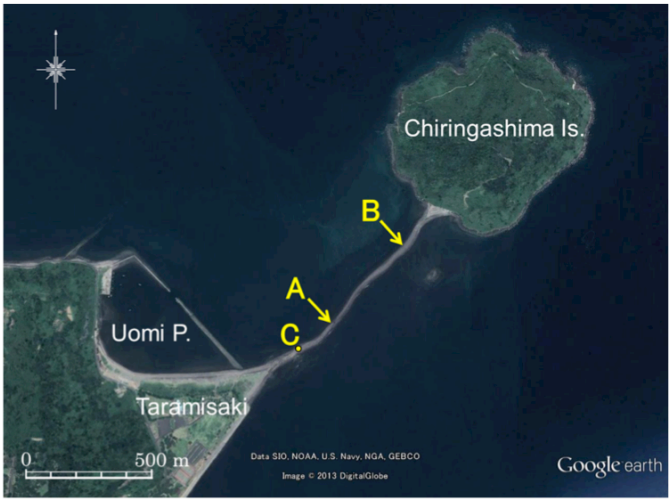

Figure 4. Satellite image of Chiringashima Island.

SITE OBSERVATION ON OYOSHIMA AND CHIRINGASHIMA ISLANDS

Sand bar of a land-tied island extending between Bentenjima and Oyoshima Islands

A site observation was carried out during low tide on April 26 and high tide on April 27 in 2013 to investigate the sand bar of a land-tied island extending between Bentenjima Island adjacent to the Ojimae fishing port, which is located in the south part of Shodoshima Island, and Oyoshima Island. In this area, two small isolated islands, namely, Nakayoshima and Shoyoshima Islands, are also located between the islands. The primary study area is the sand bar extending between the Ojimae fishing port and Oyoshima Island located 600 m south of the fishing port, as shown in Fig. 2. Bentenjima Island connects with the main island at present because of the construction of the Ojimae fishing port.

Figures 5 and 6 show a view of the sand bar extending from the mainland to Nakayoshima island, taken from the top of Bentenjima Island (A in Fig. 2) during low and high tides, facing south. On the west side of the sand bar, a seabed with a gentle slope covered with gravel extended. Although the top of the sand bar was exposed during low tide, it was immediately below the sea surface during high tide. In addition, the sand bar had developed along the eastern marginal line of a shallow gravel bed with a gentle slope. In contrast, the beach on the east side of the sand bar had a steep slope, and exposed rocks covered with seaweed were observed offshore of the sand bar, implying no sand movement. Furthermore, this sand bar had a concave shoreline on the east side.

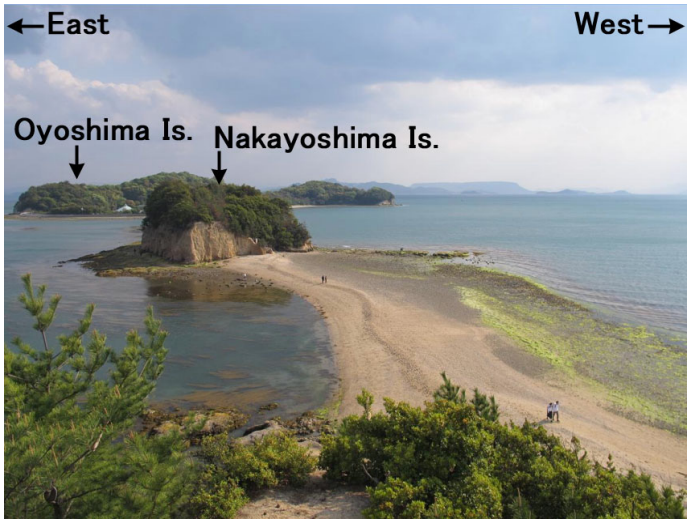

Figure 5. Oblique photograph of sand bar extending between Bentenjima and Nakayoshima Islands taken during low tide on April 26, 2013.

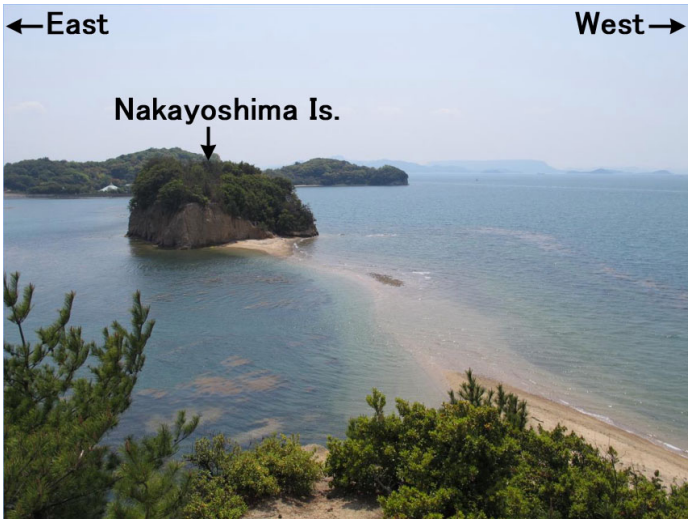

Figure 6. Oblique photograph of sand bar extending between Bentenjima and Nakayoshima Islands taken during high tide on April 27, 2013.

On Nakayoshima Island, a sea cliff and a wide wave-cut bench can be seen on the east side, in contrast to a lack of abrasion on the west side of the island, implying that the wave intensity from the east is greater than that from the west because of the longer fetch distance to the east, as shown in Figs. 1 and 2. The beach material of the sand bar was composed of well-sorted granite sand supplied from sea cliffs composed of unconsolidated granite layers.

Figure 7 shows the foreshore of the sand bar elongating from the west end of Bentenjima to Nakayoshima Islands; the foreshore slope was 1/6.3 and the materials were composed of granite coarse sand with gravel. Figure 8 shows the sea cliff and wave-cut bench formed on the eastern side of Nakayoshima Island. The sea cliff is the highest at the east end with a gradually decreasing height westward and was composed of a well-weathered granite layer. From this, it was inferred that Nakayoshima Island itself was a sand source for littoral sediment necessary for forming the land-tied island, and sand is mainly suppied from the east side of the island.

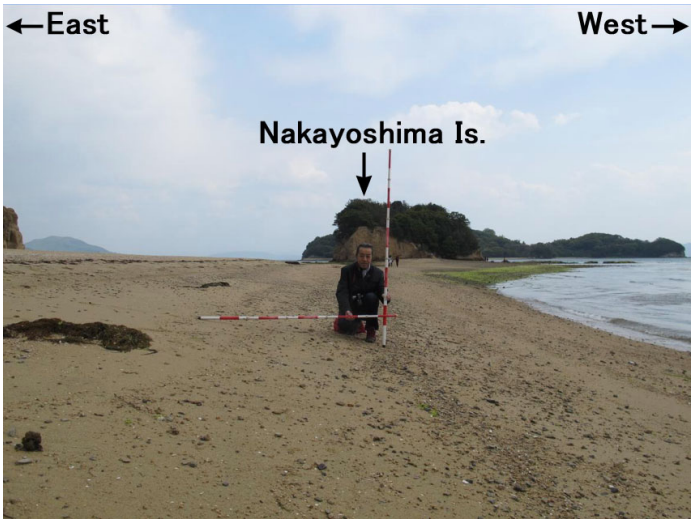

Figure 7. Foreshore slope of 1/6.3 measured at north side of Nakayoshima Island.

Figure 8. Sea cliff and wave-cut bench on east side of Nakayoshima Island.

Figure 9 shows the face of the sea cliff of Nakayoshima Island continuously extending southward with the formation of sea caves at several locations and the flat wave-cut bench. Furthermore, Fig. 10 shows a photograph of the sand bar extending toward Oyoshima Island, taken at the south end of Shoyoshima Island. The west part of this sand bar was a gravel bed with a gentle slope and a sand bar extended along the eastern edge of the gravel bed. Figure 11 shows the condition of the sand bar, taken

from the north end of Oyoshima Island (point B in Fig. 2) while looking at Shoyoshima Island. Granite sand was deposited on the gravel bed composed of andesite.

After the sand bar connects to Oyoshima Island, a small pocket beach develops in the extension of the land-tied island, as shown in Fig. 2. Considering that the shoreline of this pocket beach has a hooked shape northward, it is found that wind waves from the southwest prevail on this pocket beach. Under the wave condition, northward longshore sand transport may develop from Oyoshima Island. Figure 12 shows the south end of the pocket beach, where the unconsolidated layers of granite were eroded away under wave action, and a scarp was formed with the exposure of many roots of trees owing to erosion. In addition, at the corner of the stone-made seawall seen at the left end in Fig. 12, the seawall collapsed owing to the erosion, and granite sand was deposited on the shallow flat bed in front of the collapsed seawall, as shown in Fig. 13. A mark was left behind along the high-tide shoreline, which shows the evidence of sand movement by northward longshore sand transport, as shown by an arrow in Fig. 13. From this, sand composed of a sand bar of a land-tied island extending between Bentenjima and Oyoshima Islands was supplied not only from the sea cliffs of Nakayoshima and Shoyoshima Islands but also partly from the west side of Oyoshima Island by northward longshore sand transport.

Figure 9. Steep sea cliff and wave-cut bench of Nakayoshima Island.

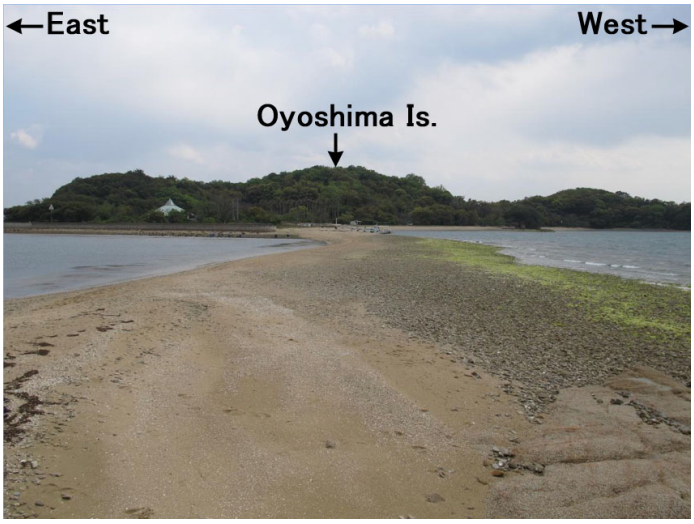

Figure 10. Sand bar extending between Shoyoshima and Oyoshima Islands.

Figure 11. Sand bar extending between Oyoshima and Shoyoshima Islands.

Figure 12. Erosion at south end of pocket beach on west shore of Oyoshima Island.

Figure 13. High water marks showing longshore sand transport turning around damaged seawall.

A sand bar of a land-tied island of Chiringashima

Chiringashima Island, which has a 3 km peripheral length, 60 ha area and an elevation of around 90 m height, is a part of the outer rim of a volcanic crater of the Ibusuki Caldera. The field observation of the sand bar of a land-tied island extending from the Ibusuki coast to Chiringashima Island was carried out on August 4, 2013. This sand bar of a land-tied island is triangular at the connection to the main land, as shown in Fig. 4, and it connects to the hooked shoreline behind the Uomi Port breakwater on the north side. In contrast, on the south side, a gently sloping revetment extends from the Ibusuki coast. Although the sand bar is approximately straight, a concave shoreline is formed around points A and B, as shown in Fig. 4, with a convex part in between. In addition, a triangular sand bar is formed immediately behind Chiringashima Island.

Figure 14 shows a photograph of a sand bar elongating to Chiringashima Island, taken from point C, from where the width of the sand bar begins to narrow, as shown in Fig. 4. The width of the sand bar narrowed with decreasing sand bar height northeast from this point. The high water marks that indicate sand movement on the beach surface were left, as denoted by the broken line. Figure 15 shows a photograph of the sand bar and high water marks of the overwash, taken at a location further northeast, approaching Chiringashima Island. Sand transported from the south side by wave action was deposited on the north side of the sand bar, while forming a steep slope, together with the traces of wave action from the northwest, implying that the sand bar received wave action from both sides.

Figure 14. High tide mark at point C on Chiringashima sand bar (south side).

Figure 15. High tide mark at point C on Chiringashima sand bar (north side).

Summary of field observations

Similar to the sand bar of a land-tied island extending between Bentenjima and Oyoshima Islands, the sand bar of a land-tied island of Chiringashima has been formed on an extremely shallow seabed, and the overwash from the northwest to the southeast sides occurs in winter with the prevailing northwest wind, whereas the overwash in the opposite direction occurs in summer, when storm waves from the Pacific Ocean are incident to Kagoshima Bay (Nagayama et al., 2009, 2010). Furthermore, sand transported to the other side of the sand bar by the overwash could be transported shoreward during the calm wave condition to recover the sand bar. Thus, the shape of a sand bar of a land-tied island is considered to be maintained in the present form with some variations, because wave action from opposite directions balance each other on average. The land-tied islands elongating from Bentenjima to Oyoshima Islands and extending to Chiringashima Island satisfy these conditions, and thus, the shapes of these sand bars have been maintained for a long time. Furthermore, although the sand bar of a land-tied island of Oyoshima is convex to the west, the formation of this convex shape is considered to be caused by the greater intensity of the waves from the east relative to that from the west because of the longer fetch distance to the east, as shown in Figs. 1 and 2.

NUMERICAL MODEL

The sand transport equation employed in this study is Eq. (1), using the expression of the wave energy flux evaluated at the breaking point, the same as in the BG model proposed by Serizawa et al. (2006) and San-nami et al. (2013). The variables in Eq. (1) are given by Eqs. (2) - (5).

$$\vec{q} = C_0 \frac{K_s P}{\tan\beta_c}\left\{\tan\beta_c \vec{e_w} - |\cos\alpha|\ \overrightarrow{\nabla Z}\right\} \qquad \left(-h_c \le Z \le h_R\right) \tag{1}$$

$$P = \varepsilon(Z)\left(EC_g\right)_b \tan\beta_w \qquad \left(\mathrm{P} \ge 0\right) \tag{2}$$

$$\tan\beta_w = dZ/dx_w \qquad \left(\tan\beta_w \ge 0\right) \tag{3}$$

$$\int_{-h_c}^{h_R} \varepsilon(Z)dZ = 1 \tag{4}$$

$$\varepsilon(Z) = \begin{cases} \dfrac{1}{h_c + h_R} & \left(-h_c \le Z \le h_R\right) \\ 0 & \left(Z < -h_c,\ Z > h_R\right) \end{cases} \tag{5}$$

Here, $\vec{q} = \left(q_x,\ q_y\right)$ is the net sand transport flux, $Z\ (x, y, t)$ is the seabed elevation with reference to the still water level ($Z = 0$), $\overrightarrow{\nabla Z} = \left(\partial Z/\partial x,\ \partial Z/\partial y\right)$ is the seabed slope vector, $\vec{e_w}$ is the unit vector of wave direction, α is the angle between the wave direction and the direction normal to the contour line, x_w is the coordinate along the direction of wave propagation, $\tan\beta_w$ is the seabed slope measured along the direction of wave propagation, $\tan\beta_c$ is the equilibrium slope of sand, and K_s is the sand transport coefficient. C_0 is the coefficient transforming the immersed weight expression to the volumetric expression ($C_0 = 1/\left\{\left(\rho_s - \rho\right)g\left(1-p\right)\right\}$; ρ is the seawater density, ρ_s is the specific gravity of sand, p is the porosity of sand, and g is the acceleration due to gravity), h_c is the depth of closure, and h_R is the berm height. $\varepsilon(Z)$ is the depth distribution of sand transport, and $(EC_g)_b$ is the wave energy flux at the breaking point.

For the calculation of the P value, another coordinate system different from that for the calculation of beach changes was used (San-nami et al., 2013; Serizawa et al., 2014), in which the x_w- and y_w-axes were taken along the wave direction and the direction normal to that, respectively. In this case, wave refraction was neglected, and waves were assumed to propagate in a straight manner while maintaining the wave incident angle. The P value was calculated using an alternate equation of Eq. (2) by introducing the cummulative form of the depth distribution of the intensity function of sediment transport. The P value calculated at point (x_w, y_w) is memorized and the P value at point (x, y) necessary for the calculation of beach changes was interpolated from the memorized value at point (x_w, y_w). By using this method, the wave-sheltering effect due to the island or the sand bar is taken into account in

the P value, although wave refraction is neglected. The details of the calculation method were described by San-nami et al. (2013) and Serizawa et al. (2014).

The mesh intervals of Δx_w and Δy_w are the same as those of Δx and Δy. Here, Δx and Δy are the mesh intervals of the coordinate system for the calculation of beach changes, and we assumed the equivalent condition of $\Delta x = \Delta y$. The beach changes were calculated by explicitly solving the continuity equation ($\partial Z/\partial t + \nabla \bullet \vec{q} = 0$) on the staggered meshes using the sand transport fluxes obtained from Eq. (1). The P value, which is subject to change with the propagation of waves, was recalculated at every calculation step of beach changes.

CALCULATION CONDITIONS

Irregular waves were assumed to be incident from the upper and lower sides of the calculation domain, and the topographic changes associated with the elongation of a sand bar of a land-tied island were predicted using the BG model. Two sand sources were placed on both sides of the calculation domain in Cases 1 and 2, which had different probabilities of the occurrence of waves from two opposite directions, 1:1 and 1:0.5 in Cases 1 and 2, respectively, as shown in Fig. 16. In Case 3, two sand sources were alternately placed on both sides of the calculation domain with the same probability of the occurrence of waves from two opposite directions as in Case 1. In Case 4, a sand source modeling a sea cliff, from which sand was supplied from Nakayoshima Island, was set at the center of the calculation domain with three small islands on each side of the sand source. To model the supply of sand from the sea cliffs of the island, the sand deficit was supplied in each step to maintain the topography of the sand source over time, even though sand is transported away from the sand source at each step. This sand source is considered to be an island because of its wave-sheltering effect.

The wave direction at each step was randomly determined given the probability of the occurrence of the wave direction, as described by San-nami et al. (2013). As the probability distribution of the occurrence of waves incident from two opposite directions, the energy distribution for multidirectional irregular waves with a directional spreading parameter of $S_{max} = 10$ was used. In the calculation, a flat shallow body of water with a constant depth of 3 m was assumed. The depth of closure and equilibrium slope were assumed to be $h_c = 3$ m and 1/10, respectively, which was equal to the initial slope. The calculation domain was a rectangular area with 600 m length in the longshore and cross-shore directions in Cases 1, 2 and 3, and 2000 and 500 m in longshore and cross-shore directions in Case 4. The calculation domain was discretized by 10 m meshes. The time interval was set to $\Delta t = 2$ hr and the total number of calculation steps was 2×10^4. Sand transport was set to zero at the boundaries. Table 1 shows the calculation conditions.

The calculation was carried out under the condition that waves were incident with a probability from all the directions on both sides of a sand bar of a land-tied island. Therefore, the wave-sheltering effect increased around an island or the sand bar, which enhanced the sand deposition in the wave-shelter zone, and in turn, sand deposition further increased the wave-sheltering effect.

Table 1. Calculation conditions.

Incident wave height H	1 m
Berm height h_R	1 m
Depth of closure h_c	3 m
Equilibrium slope $\tan\beta_c$	1/10
Coefficients of sand transport	Coefficient of longshore sand transport K_s = 0.2 Coefficient of cross-shore sand transport $K_n = K_s$
Mesh size	$\Delta x = \Delta y$ = 10 m
Time interval	Δt = 2 hr
Duration of calculation	80,000 hr (40,000 step)
Boundary conditions	Shoreward and landward ends $q_x = 0$ Right and left boundaries $q_y = 0$

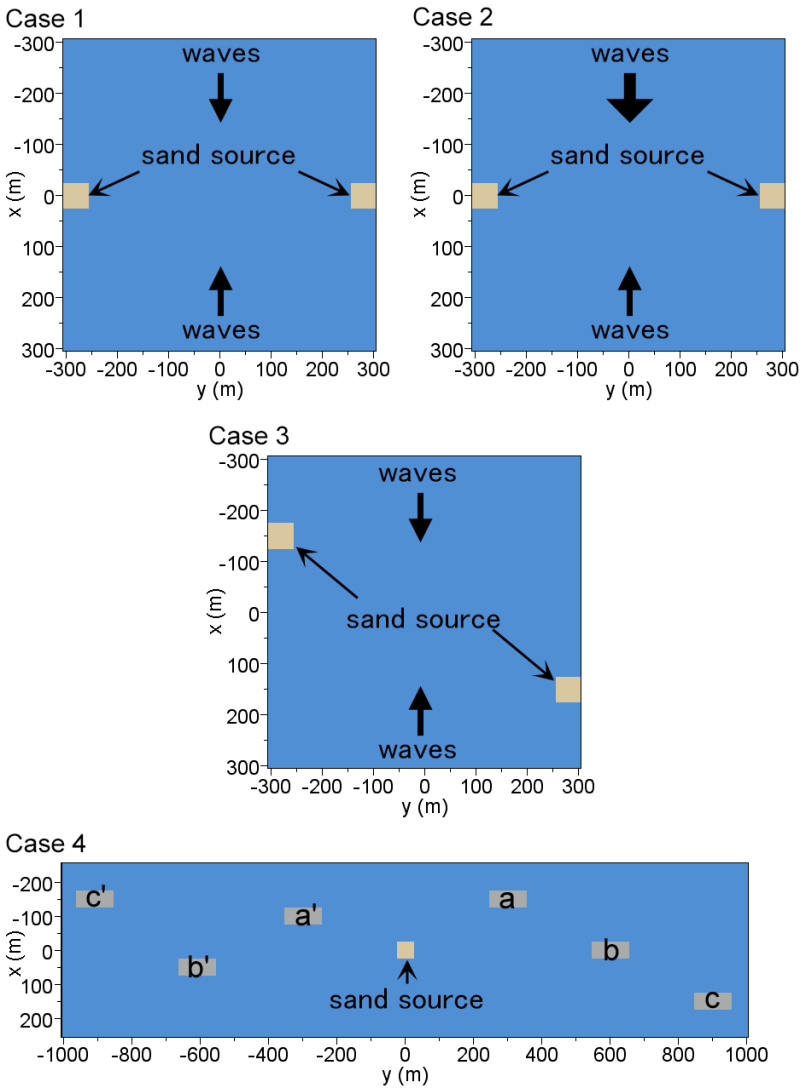

Figure 16. Calculation conditions of four cases.

RESULTS

When sand sources were set on both sides of the calculation domain, and irregular waves with a significant wave height of 1 m were incident from the upper and lower sides of the calculation domain with the same probability of occurrence as in Case 1, a pair of cuspate forelands extended and then a straight sand bar was formed, as shown in Fig. 17. In Case 2, in which the probability of occurrence was asymmetric (1:0.5), two cuspate forelands oriented downward were formed at the initial stage. They approached each other, and after 8×10^3 hr, a sand bar was formed with a convex upper shoreline, as shown in Fig. 18. It was found that when the probability of occurrence of waves was different, the effect of the asymmetric wave incidence was left in the asymmetric form of a cuspate foreland and a land-tied island. These results are in good agreement with the measured results, as shown in Fig. 5, where the sand bar connecting Bentenjima and Oyoshima Islands had a concave shape on the east side, implying that the wave intensity from the east is greater than that from the west.

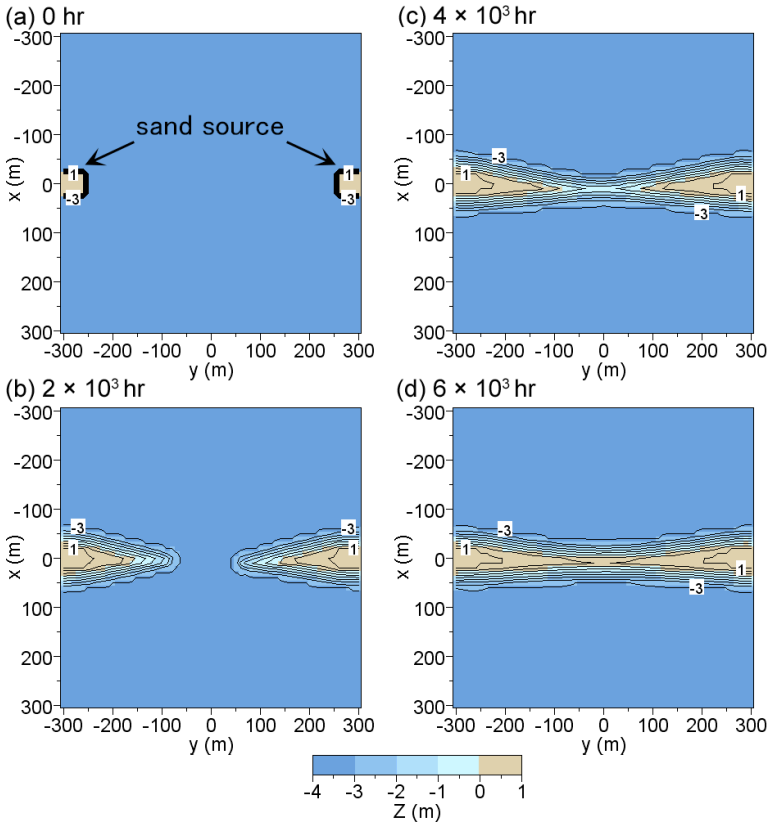

Figure 17. Calculation results of Case 1.

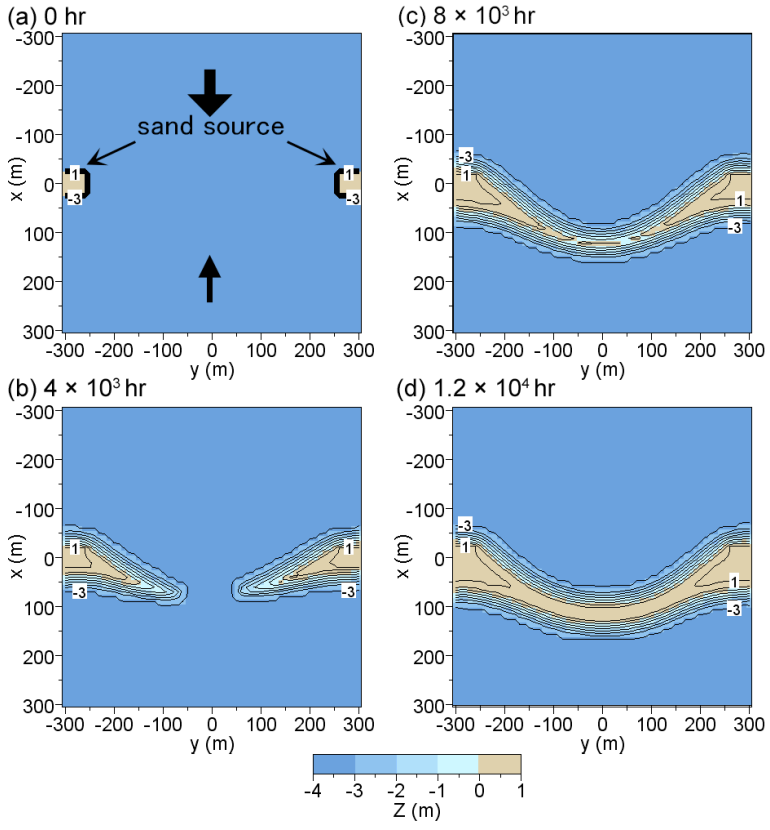

Figure 18. Calculation results of Case 2.

When two sand sources were alternately placed on both sides of the calculation domain as in Case 3, the cuspate forelands on both sides pulled at each other owing to the wave-sheltering effect and the sand bars connected. Finally, an oblique cuspate foreland was formed after 2×10^4 hr, as shown in Fig. 19.

In Case 4, we predicted the elongation of a sand bar, as shown in Fig. 20, including land-tied islands such as those near Oyoshima Island, as shown in Fig. 2. After 8×10^3 hr, a slender sand bar extended from the sand source to behind the islands owing to the wave-sheltering effect of islands a and a'. After 1.6×10^4 hr, the sand deposition zone extended toward islands b and b'. After 2.4×10^4 hr, the tip of the sand bar reached the ends of islands b and b', and after 3.2×10^4 hr, the sand bar extended beyond islands b and b'. Finally, after 4×10^4 hr, the sand bar reached islands c and c' located at both ends of the calculation domain. The connection of the small islands by a slender sand bar convincingly explains the elongation of the sand bar connecting Oyoshima Island.

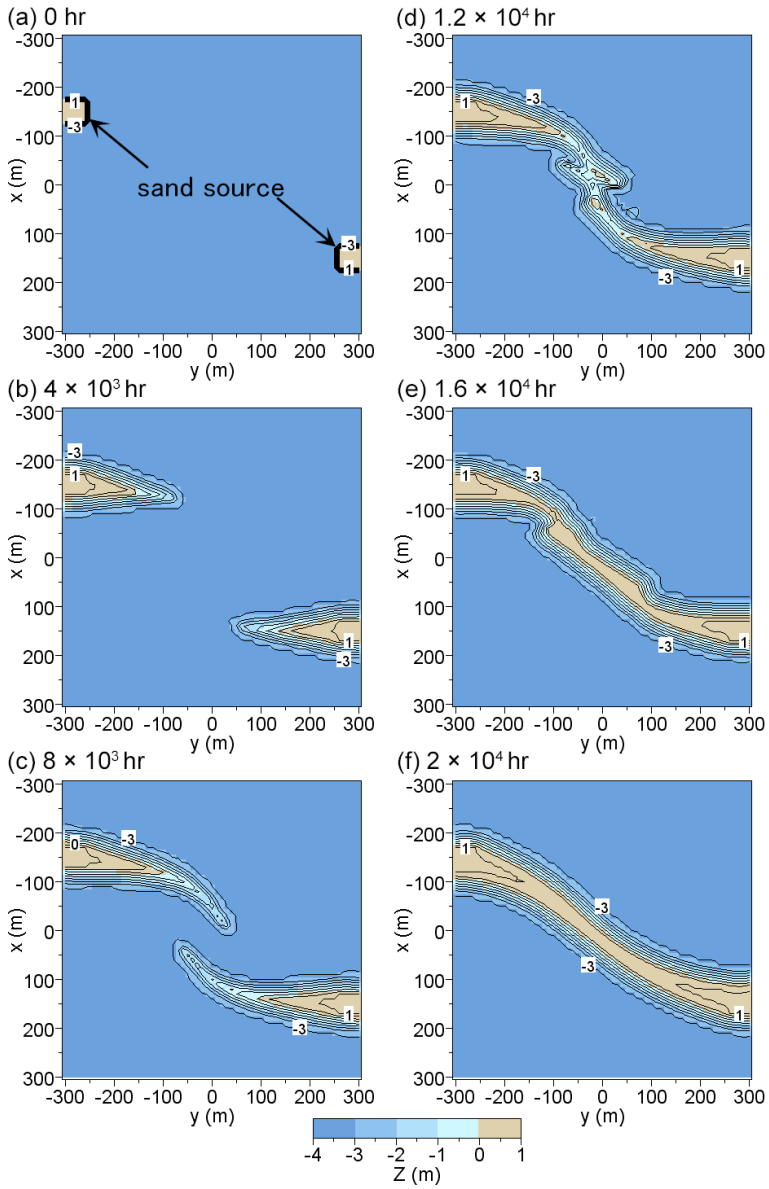

Figure 19. Calculation results of Case 3.

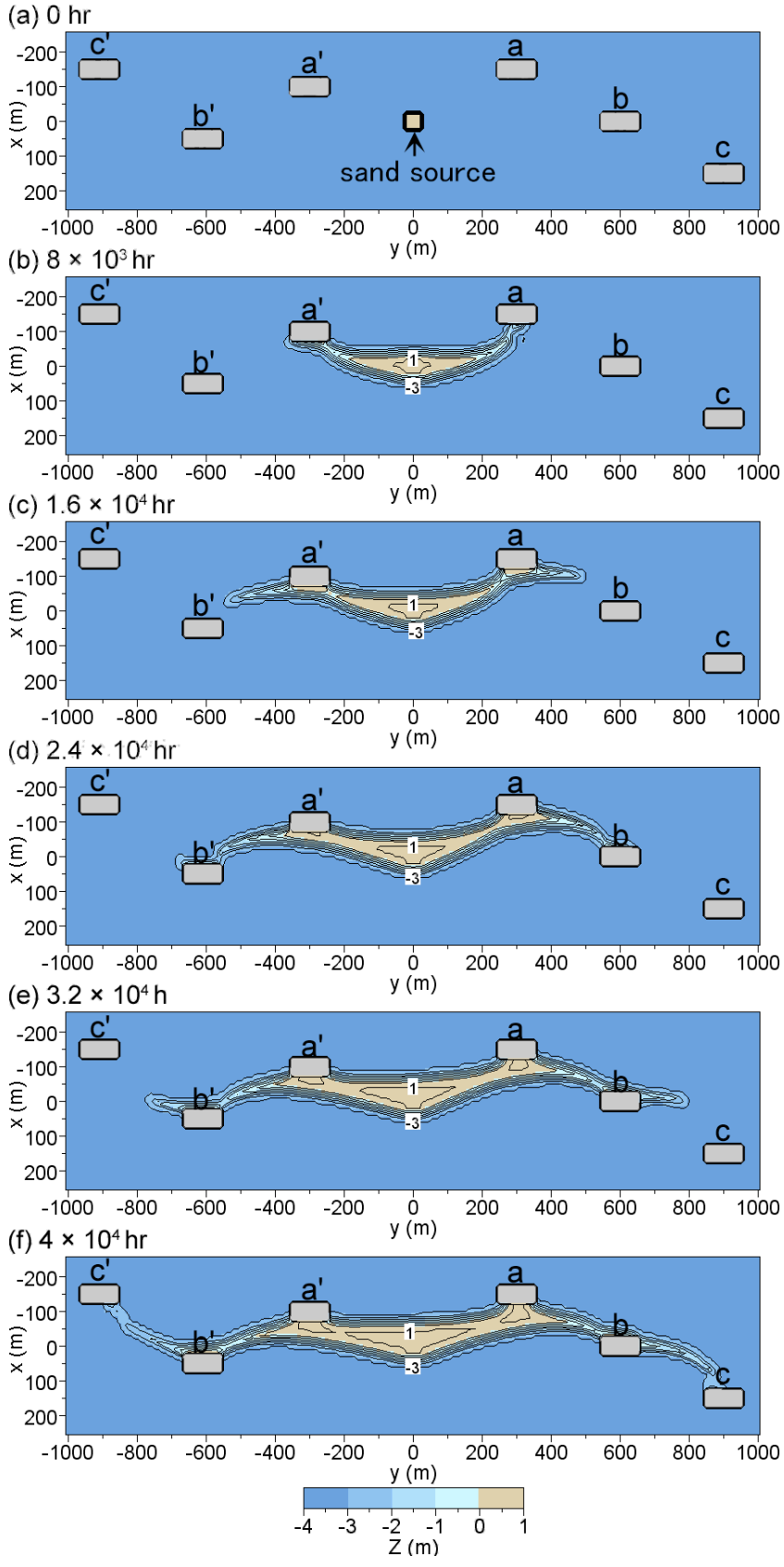

Figure 20. Calculation results of Case 4.

CONCLUSIONS

Field observations were carried out at the sand bar of two land-tied islands of Oyoshima and Chiringashima. Then, we developed a numerical model for predicting the elongation of a sand bar of a land-tied island using the BG model. The elongation of a sand bar connecting land-tied islands was successfully predicted using the BG model when the wave direction at each step was randomly determined given the probability of the occurrence of the wave direction, as described by San-nami et al. (2013). It was concluded that the wave-sheltering effect of the islands and the shallowness of the body of water were important factors for the extension of a slender sand bar and the formation of a land-tied island.

REFERENCES

Nagayama, A., Yamaguchi, H., Chaya, A., Tanaka, R., Nakamura, K. and Asano, T. 2009. Study on emerging and submerging processes of a tombolo at Chiringashima Island, Ibusuki City, *J. JSCE, Ser. B2 (Coastal Engineering)*, Vol. 65, No.1, pp. 586-590. (in Japanese)

Nagayama, A., Taniyama, M., Kawakami, K. and Asano, T. 2010. Study on deformation process of a tombolo throughout a whole year at Chiringashima Island, Ibusuki City, *J. JSCE, Ser. B2 (Coastal Engineering)*, Vol. 66, No.1, pp. 156-160. (in Japanese)

Serizawa, M., Uda, T., San-nami, T. and Furuike, K. 2006. Three-dimensional model for predicting beach changes based on Bagnold's concept, *Proc. 30th ICCE*, pp. 3155-3167.

Serizawa, M., Miyahara, S. and Uda, T. 2014. Interaction between two circular sandy islands on flat shallow seabed owing to waves, *Proc. 34th ICCE*. (in press)

San-nami, T., Uda, T., Serizawa, M. and Miyahara, S. 2013. Prediction of devastation of natural coral cay by human activity, *Proc. Coastal Dynamics 2013*, Paper No. 138, pp. 1427-1438.